Marine Modelling Report

Outer Loch Shell

CAR/L/1120220 (Caolas a Deas East)
CAR/L/1120218 (Caolas a Deas West)
April 2024

Mowi Scotland

OFFICE
Mowi, Farms Office, Glen Nevis Business Park
PH33 6RX Fort William

POSTAL
Mowi, Farms Office, Glen Nevis Business Park
PH33 6RX Fort William

PHONE

FAX
-

MAIL
environment@mowi.com

WEB
http://mowiscotland.co.uk

CONTENTS

Page

1. INTRODUCTION 6

2. MODEL DESCRIPTION 6

3. CONFIGURATION AND BOUNDARY FORCING FOR LOCH SHELL 7

4. MODEL CALIBRATION AND VALIDATION 10

4.1 Simulation Periods 10

4.1.1 Near-Surface Current Measurements 10

4.2 Calibration: 06 October – 29 November 2023 (ID424) 11

4.3 Validation: 09 February – 07 May 2021 (ID367) 14

4.4 Validation: 24 June – 10 September 2020 (ID346) 17

4.5 Validation: 10 September – 08 November 2020 (ID357, ID358) 20

4.5.1 ID357 20

4.5.2 ID358 23

5. MODELLED FLOW FIELDS 26

6. MODEL EVALUATION AGAINST DYE & DROGUE TRACK DATA 28

7. REFERENCES 30

LIST OF FIGURES

Figure 1. Locations of the Caolas a Deas East and West sites in Loch Shell (top) and the layout of the 160m pens (O) bottom. The boundary of the planning area is indicated (▬). 7

Figure 2. The mesh and domain of the East Lewis model. The pen locations in Loch Shell are marked (●) and freshwater input locations are also indicated (→). 8

Figure 3. The unstructured mesh around the Caolas a Deas sites, with the pen locations indicated (●). The ADCP deployment locations ID367 and ID424 (▲) and locations of freshwater discharge (→) are also indicated. 8

Figure 4. Multibeam survey of bathymetry around Caolas a Deas farm sites from December 2020 (left). Model water depths (H, m) in the model domain (right), incorporating the multibeam data. The proposed cage locations are indicated (●). 9

Figure 5. Western and northern point source (Figure 2) climatological river flows into Loch Shell used in the modelling. 10

Figure 6. Comparison between observed and modelled sea surface height from September – December 2020 (ID360) using model parameter values from Table 1. Both the full record (left) and a subset of 15 days (right) are shown. Observed data are in blue, model results in red. 12

Figure 7. Comparison between observed and modelled East (left) and North (right) components of velocity at the ADCP location for October – November 2023 (ID424) at three depths, 2.5 m (top), 6.0 m and 10.0m (bottom) relative to the moving sea surface. Observed data are in blue, model results in red. 13

Figure 8. Histograms of observed and modelled speed (left) and direction (right) at the ADCP location for October – November 2023 (ID424) at three depths, 2.5 m (top), 6.0 m (middle) and 10.0m (bottom) relative to the moving sea surface. Observed data are in blue, model results in red. 13

Figure 9. Scatter plot of observed and modelled velocity at the ADCP location for October – November 2023 (ID424) at three depths, 2.5 m (top), 6.0 m (middle) and 10.0m (bottom) relative to the moving sea surface. Observed data are in blue, model results in red. 14

Figure 10. Comparison between observed and modelled sea surface height from 09 February – 07 May 2021 (ADCP deployment ID367) using model parameter values from Table 1. Both the full record (left) and a subset of 15 days (right) are shown. Observed data are in blue, model results in red. 15

Figure 11. Comparison between observed and modelled East (left) and North (right) components of velocity at the ADCP location for 15 days in February 2021 (ID367) at three depths, 7.9 m, 17.9 m and 43.9 m. Observed data are in blue, model results in red. 15

Figure 12. Histograms of observed and modelled current speed (left) and direction (right) at the ADCP location from 09 February – 07 May 2021 (ID367) at three depths, 7.9 m, 17.9 m and 43.9 m. Observed data are in blue, model results in red. 16

Figure 13. Scatter plot of observed and modelled velocity at the ADCP location from 09 February – 07 May 2021 (ID367) at three depths, 7.9 m, 17.9 m and 43.9 m. Observed data are in blue, model results in red. 17

Figure 14. Comparison between observed and modelled sea surface height from 24 June – 10 September 2020 (ADCP deployment ID346) using model parameter values from Table 1. Both the full record (left) and a subset of 15 days (right) are shown. Observed data are in blue, model results in red. 18

Figure 15. Comparison between observed and modelled East (left) and North (right) components of velocity at the ADCP location from 24 June – 10 September 2020 (ADCP deployment ID346) at three depths, 6.9m, 17.9 m and 48.9 m. Observed data are in blue, model results in red. 18

Figure 16. Histograms of observed and modelled current speed (left) and direction (right) at the ADCP location from 24 June – 10 September 2020 (ADCP deployment ID346) at three depths, 6.9m, 17.9 m and 48.9 m. Observed data are in blue, model results in red. 19

Figure 17. Scatter plot of observed and modelled velocity at the ADCP location from 24 June – 10 September 2020 (ADCP deployment ID346) at three depths, 6.9m, 17.9 m and 48.9 m. Observed data are in blue, model results in red. 20

Figure 18. Comparison between observed and modelled sea surface height from ID357 using model parameter values from Table 1. Both the full record (left) and a subset of 15 days (right) are shown. In the latter, the observed data are in blue, model results in red. 21

Figure 19. Comparison between observed and modelled East (left) and North (right) components of velocity at the ADCP from 10 September – 08 November 2020 (ID357) at three depths: 7.7m (top), 16.7 m (middle) and 48.7m (bottom). Observed data are in blue, model results in red. 22

Figure 20. Histograms of observed and modelled speed (left) and direction (right) at the ADCP location from 10 September – 08 November 2020 (ID357) at three depths: 7.7m (top), 16.7 m (middle) and 48.7m (bottom). Observed data are in blue, model results in red. 22

Figure 21. Scatter plot of observed and modelled velocity at the ADCP location from 10 September – 08 November 2020 (ID357) at three depths: 7.7m (top), 16.7 m (middle) and 48.7m (bottom). Observed data are in blue, model results in red. 23

Figure 22. Comparison between observed and modelled sea surface height from ID358 using model parameter values from Table 1. Both the full record (left) and a subset of 15 days (right) are shown. In the latter, the observed data are in blue, model results in red. 24

Figure 23. Comparison between observed and modelled East (left) and North (right) components of velocity at the ADCP location from 10 September – 08 November 2020 (ID358) at three depths: 7.4m (top), 14.4 m (middle) and 46.4m (bottom). Observed data are in blue, model results in red. 25

Figure 24. Histograms of observed and modelled speed (left) and direction (right) at the ADCP location from 10 September – 08 November 2020 (ID358) at three depths: 7.4m (top), 14.4 m (middle) and 46.4m (bottom). Observed data are in blue, model results in red. 25

Figure 25. Scatter plot of observed and modelled velocity at the ADCP location from 10 September – 08 November 2020 (ID358) at three depths: 7.4m (top), 14.4 m (middle) and 46.4m (bottom). Observed data are in blue, model results in red. 26

Figure 26. Modelled flood (top) and ebb (bottom) sub-surface (model layer 2) current vectors during spring tides on 18th and 15th October 2023 respectively. For clarity, only 20% of the model vectors are shown. Pen locations are indicated (O). 27

Figure 27. Modelled mean (residual) sub-surface (model layer 2) current vectors averaged over the full simulation from 6th October – 30th November 2023. For clarity, only 20% of the model vectors are shown. Pen locations are indicated (O). 28

Figure 28. Observed (points) and modelled (solid lines) dye tracks for the four successful dye releases at Caolas a Deas on the 23rd July 2020. The dye release locations (■) and pen locations (●) are indicated. 29

Figure 29. Observed (points) and modelled (solid lines) drogue tracks from the five releases at Caolas a Deas on 23rd July 2020. The different shaped points (○, ◊, □, Δ) represent

individual drogues, while the colouring indicates the release number. The drogue release locations (■) and pen locations (●) are indicated. 30

LIST OF TABLES

Table 1. Parameter values chosen for the FVCOM model during the calibration simulations. 11
Table 2. Model performance statistics for sea surface height (SSH), and East and North velocity at the ADCP location for October – November 2023 (ID424) at three depths, 2.5 m, 6.0 m and 10.0m relative to the moving sea surface......12
Table 3. Model performance statistics for sea surface height (SSH), and East and North velocity at the ADCP location from 09 February – 07 May 2021 (ID367) at three depths, 7.9 m, 17.9 m and 43.9 m......16
Table 4. Model performance statistics for sea surface height (SSH), and East and North velocity at the ADCP location from 24 June – 10 September 2020 (ADCP deployment ID346) at three depths, 6.9m, 17.9 m and 48.9 m......19
Table 5. Model performance statistics for sea surface height (SSH) and East and North velocity at the ADCP location from 10 September – 08 November 2020 (ID357) at three depths (7.7 m, 16.7 m and 48.7 m)......21
Table 6. Model performance statistics for sea surface height (SSH) and East and North velocity at the ADCP location from 10 September – 08 November 2020 (ID358) at three depths (7.4 m, 14.4 m and 46.4 m)......24
Table 7. Details of the dye releases undertaken at Caolas a Deas in July 2020. 28
Table 8. Details of the drogue releases undertaken at Caolas a Deas in outer Loch Shell in July 2020......29

1. Introduction

This report has been prepared by Mowi Scotland Ltd. to meet the requirements of the Scottish Environment Protection Agency (SEPA) for an application to use topical sealice veterinary medicines at the **Caolas a Deas East** and **West** marine salmon farms in **Loch Shell** (Figure 1). The application uses coupled hydrodynamic and particle tracking modelling to describe the dispersion of bath treatments in order to determine EQS-compliant quantities for the current site biomass and equipment. The modelling procedure follows as far as possible guidance presented by SEPA in December 2023 (SEPA, 2023). This report describes the configuration, calibration and validation of the hydrodynamic model used in the application. The dispersion modelling for each site is described in separate reports (Mowi 2024a, b).

2. Model Description

The hydrodynamic model used was FVCOM (Finite Volume Community Ocean Model), a prognostic, unstructured-grid, finite-volume, free-surface, 3-D primitive equation coastal ocean circulation model developed by the University of Massachusetts School of Marine Science and the Woods Hole Oceanographic Institute (Chen et al., 2003). The model consists of equations describing the evolution and conservation of momentum, temperature, salinity and turbulence parameters, the latter using a turbulence closure submodel. The horizontal grid is comprised of unstructured triangular cells and the irregular bottom is presented using generalized terrain-following coordinates. The Mellor-Yamada level 2.5 and General Ocean Turbulent Model (GOTM, Burchard, 2002) are included as optional vertical turbulent closure schemes. Horizontal viscosity and diffusivity was constant, with a coefficient value c_s. FVCOM is solved numerically by a second-order accurate discrete flux calculation in the integral form of the governing equations over an unstructured triangular grid. This approach combines the best features of finite-element methods (grid flexibility) and finite-difference methods (numerical efficiency and code simplicity) and provides a much better numerical representation of both local and global momentum, mass, salt, heat, and tracer conservation. The ability of FVCOM to accurately solve scalar conservation equations in addition to the topological flexibility provided by unstructured meshes and the simplicity of the coding structure has make FVCOM ideally suited for many coastal and interdisciplinary scientific applications, such as typically found in Scotland. The mesh flexibility allows greater spatial resolution in near-shore areas without excessive computational demand.

The model is forced by a tidal condition along the open boundary, and by frictional stresses at the surface and seabed. At the seabed, the frictional stress, $\boldsymbol{\tau}_b$, is calculated using a quadratic equation where:

$$\tau_b = \rho C_D \boldsymbol{U}|\boldsymbol{U}| \quad (1)$$

where ρ = 1025 kg m^{-3} is the water density, **U** is the velocity in the layer closest to the seabed. The drag coefficient, C_D, is calculated from the bed roughness lengthscale, z_0, using:

$$C_D = \left(\frac{\kappa}{\ln\left(\frac{z_b + z_0}{z_0}\right)}\right)^2 \quad (2)$$

where κ=0.4 is von Karman's constant, and z_b is the height above the bed of the lowest velocity point. The value of z_0 was varied during calibration to provide the best fit to observations of sea level and velocity.

Wind forcing is applied as a surface stress calculated from hourly wind speed and direction. Wind stress is calculated from the wind velocity by a standard quadratic relation:

$$\tau_x = \rho_a C_W u W \quad (3a)$$
$$\tau_y = \rho_a C_W v W \quad (3b)$$

where (u,v) are the East and North components of wind velocity respectively, W is the wind speed ($W = [u^2+v^2]^{½}$), ρ_a is the density of air, and the surface drag coefficient C_W is calculated following Large and Pond (1981).

In the vertical, the Mellor-Yamada level 2.5 turbulence closure scheme was used (Mellor and Yamada, 1982).

3. Configuration and Boundary Forcing for Loch Shell

The Caolas a Deas East and West sites are situated in Loch Shell in the Western Isles (Figure 1). The unstructured mesh used in the model covered Loch Shell and adjacent coastal waters (Figure 2). Model resolution was enhanced in the Loch Shell region particularly around the Mowi site at Shell (Figure 3).

Figure 1. Locations of the Caolas a Deas East and West sites in Loch Shell (top) and the layout of the 160m pens (○) bottom. The boundary of the planning area is indicated (—).

The spatial resolution of the model varied from about 25 m in some inshore waters to about 450 m along the open boundary. The mesh was refined down to about 45 – 50 m in the area of the 160 m circumference (51 m diameter) pens. In total, the model consisted of 37,604 nodes and 71,795 triangular elements.

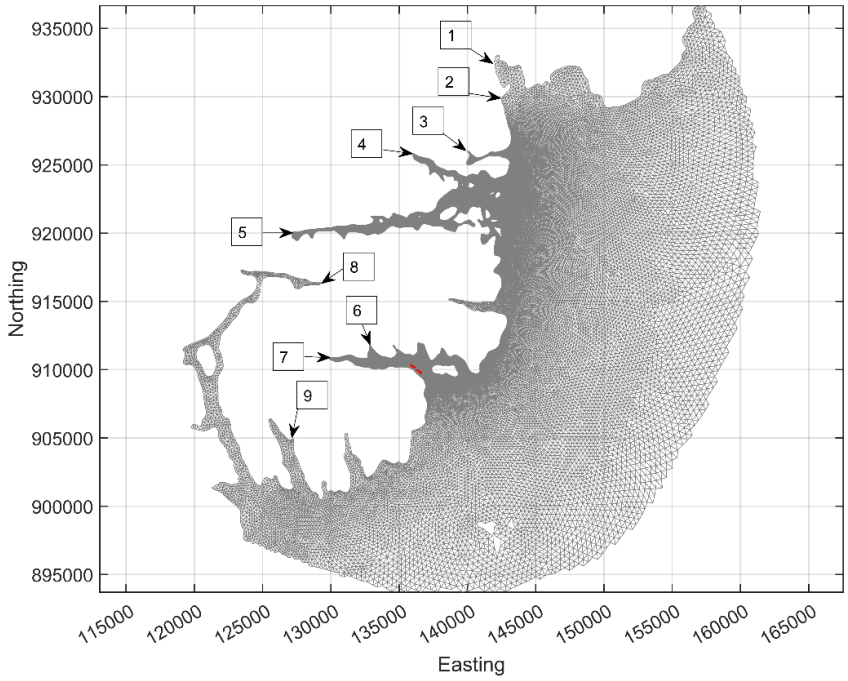

Figure 2. The mesh and domain of the East Lewis model. The pen locations in Loch Shell are marked (●) and freshwater input locations are also indicated (→).

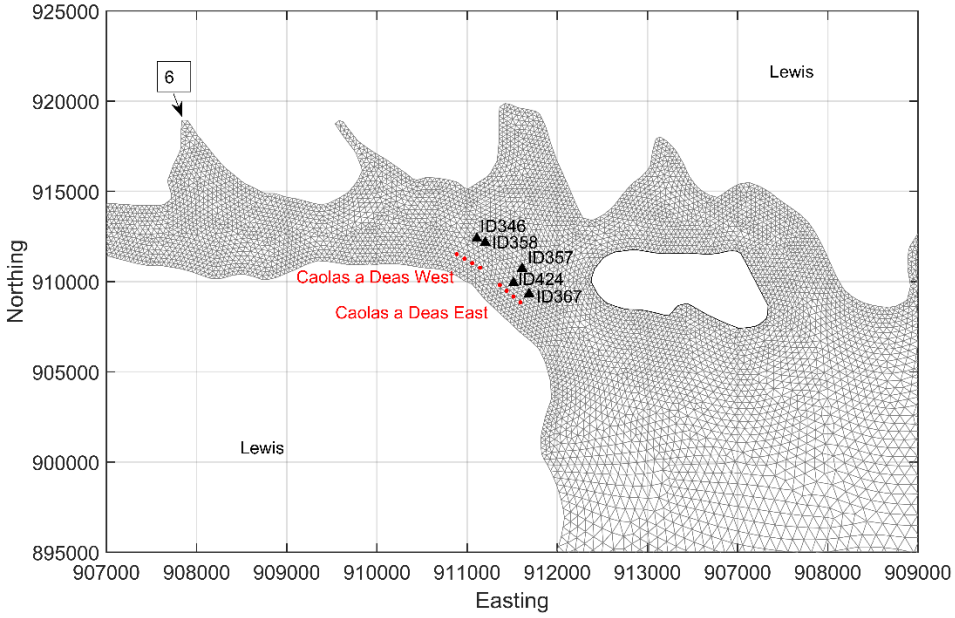

Figure 3. The unstructured mesh around the Caolas a Deas sites, with the pen locations indicated (●). The ADCP deployment locations ID367 and ID424 (▲) and locations of freshwater discharge (→) are also indicated.

Model bathymetry was taken from the UK Hydrographic Office (UKHO 2024) data portal, supplemented by a multibeam survey undertaken in June 2021 (Figure 4).

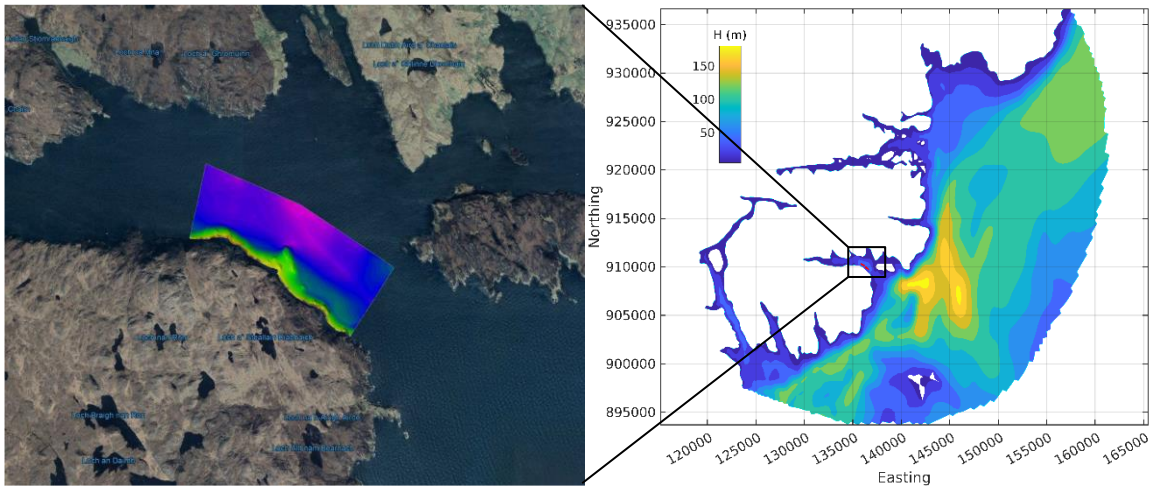

Figure 4. Multibeam survey of bathymetry around Caolas a Deas farm sites from December 2020 (left). Model water depths (H, m) in the model domain (right), incorporating the multibeam data. The proposed cage locations are indicated (●).

The model was forced along its open boundary by time series of sea surface height (SSH) at each boundary node for the relevant simulation periods; FVCOM appears to perform better when boundary forcing is applied as a time series rather than when tidal constituents are used. The SSH time series were generated using the RiCOM hydrodynamic model (Walters and Casulli, 1998; Gillibrand et al., 2016) on the Scottish Shelf Model ECLH grid (Price et al., 2016), which was, in turn, forced by eight tidal constituents (O_1, K_1, Q_1, P_1, M_2, S_2, N_2, K_2) taken from the full Scottish Shelf model (SSM).

Spatially- and temporally-varying wind speed and direction data were taken from the Weather Research and Forecast (WRF) model results, deployed operationally as part of the WestCOMS modelling system (Aleynik et al., 2016). The WRF model has a higher spatial resolution (approximately 1.5') than the ECMWF ERA5 dataset (resolution 15'), and provided better quality data for this inshore region. The data for the required simulation periods were downloaded and interpolated spatially onto the model mesh element centre locations.

Stratification is expected to be moderate in this location and the model was run in 3D baroclinic mode. Ten layers in the vertical (eleven sigma levels) were used in the simulations, with layers concentrated near the surface and seabed. The sigma levels used were:

$$\sigma = [0.00\ -0.02\ -0.08\ -0.16\ -0.32\ -0.50\ -0.68\ -0.84\ -0.92\ -0.98\ -1.00]$$

Climatological river flow data were used, taken from the Scottish Shelf Model climatology (de Dominicis et al., 2018). Nine freshwater discharges into the model domain were specified (Figure 2), with two going directly into Loch Shell. The annual climatological river flows into Loch Shell are shown in Figure 5.

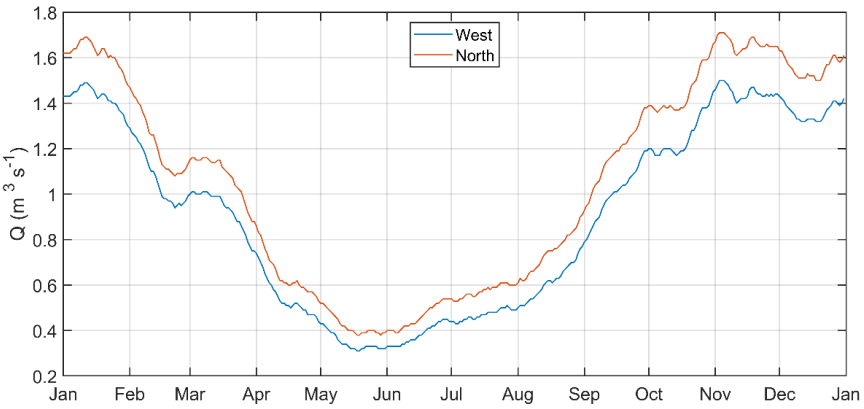

Figure 5. Western and northern point source (Figure 2) climatological river flows into Loch Shell used in the modelling.

4. Model Calibration and Validation

4.1 Simulation Periods

The hydrodynamic model was calibrated against current data and seabed pressure data, measured in the Outer Loch Shell area using Acoustic Doppler Current Profilers (ADCP, Figure 3). Data are available from:

(i) Calibration: 06 October – 29 November 2023 (ID424)
(ii) Validation: 09 February – 07 May 2021 (ID367)
(iii) Validation: 24 June – 10 September 2020 (ID346)
(iv) Validation: 10 September – 08 November 2020 (ID357, ID358)

In total, the data extended over 330 days. The model was run in 3D, and calibration was performed primarily by adjusting the bed roughness length scale, z_0, and the horizontal viscosity/diffusivity coefficient, c_s, to obtain the best fit against the sea surface height and current data. When the best comparison with the calibration data was achieved, the parameter set was tested without further adjustment against the validation datasets.

4.1.1 Near-Surface Current Measurements

The first deployment listed above (ID424) utilised a Nortek Signature 1000 ADCP instrument (Nortek, 2023). The objective of these measurements was to more accurately measure the currents in the near-surface region of the water column, where bath medicines are applied and disperse following traditional tarp treatments. The Nortek Signature 1000 is a high frequency (1 MHz) ADCP, allowing smaller cell sizes (0.2 – 2.0 m) and higher frequency sampling. The instrument was deployed at mid-depth, *ca.* 16.5 m below mean sea level (MSL), meaning that less of the sub-surface water column was lost to side-lobe reflections; measurements were made to within about 2 m of the water surface.

These data were processed in two ways:
1. The near-surface cell was selected in the usual way, namely as the shallowest cell which contains valid data throughout the deployment. As for standard deployments,

this cell was at a depth of a few metres below the lowest measured sea surface height. Given that spring tides in the area have a range of about 4.5 – 5.0 m, the near-surface cell selected in this manner was about 4.5 m below MSL. This is only just within the 0 – 5 m depth water column in which bath medicine dispersion occurs; when the SSH is positive (above MSL) the measured currents will likely lie below the actual near-surface layer in which dispersion is taking place.

2. To improve the estimation of currents in the near-surface layer (0 – 5 m depth), velocity data was extracted from a fixed depth (e.g. 2.5 m) relative to the moving water surface (by "surface tracking"). This provided a more accurate estimate of current speed and direction affecting dispersing patches of bath medicine in the top 5 m of the water column, accounting for tidal oscillations in the sea surface height throughout the deployment. The current speed and direction obtained by this approach were used to estimate the 3-hour mixing zone.

Although the data were processed and analysed using both approaches, to avoid confusion only the results from the second approach are used and presented here. The results are consistent with those obtained from the standard approach, providing confidence that the "surface-tracking" approach produced valid data.

Model performance was assessed using three metrics: the mean absolute error (MAE), the root-mean-square error (RMSE) and the model skill (d_2). The first two are standard measures of model accuracy; the third, d_2, is taken from Willmott et al. (1985) and lies in the range $0 \leq d_2 \leq 1$, with $d_2 = 0$ implying zero model skill and $d_2 = 1$ indicating perfect skill.

4.2 Calibration: 06 October – 29 November 2023 (ID424)

The calibration used observed depth and current velocity from ID424 locations to compare with modelled sea surface height (SSH) and velocity. The model was calibrated by varying the value of the bed roughness lengthscale, z_0, and the horizontal viscosity/diffusivity coefficient, c_s. Simulations were performed with a range of values of both parameters. After a number of simulations, a final parameter set was selected (Table 1).

Table 1. Parameter values chosen for the FVCOM model during the calibration simulations.

Parameter Description	Value
Bed roughness lengthscale, z_0 (m)	0.01
Horizontal viscosity coefficient, c_s ($m^2\ s^{-1}$)	1.0
Number of vertical layers	10
Barotropic time step (s)	0.5
Baroclinic time step (s)	5.0

The analysis for this deployment is slightly different in that observed data and the corresponding model results are extracted at fixed depths relative to the moving sea surface. The instrument was deployed at about 16.5 m below mean sea level (MSL); depths selected for model-data comparison were 2.5 m, 6.0 m and 10.0 m below the moving sea surface.

At the ADCP location, the sea surface height was accurately modelled, with model skill of 1.00 (Figure 6, Table 2). The mean absolute error (MAE) and root-mean-square error (RMSE)

values of 0.11 m and 0.14 m respectively are about 2.4% and 3.1% of the spring tide range (4.5 m) respectively.

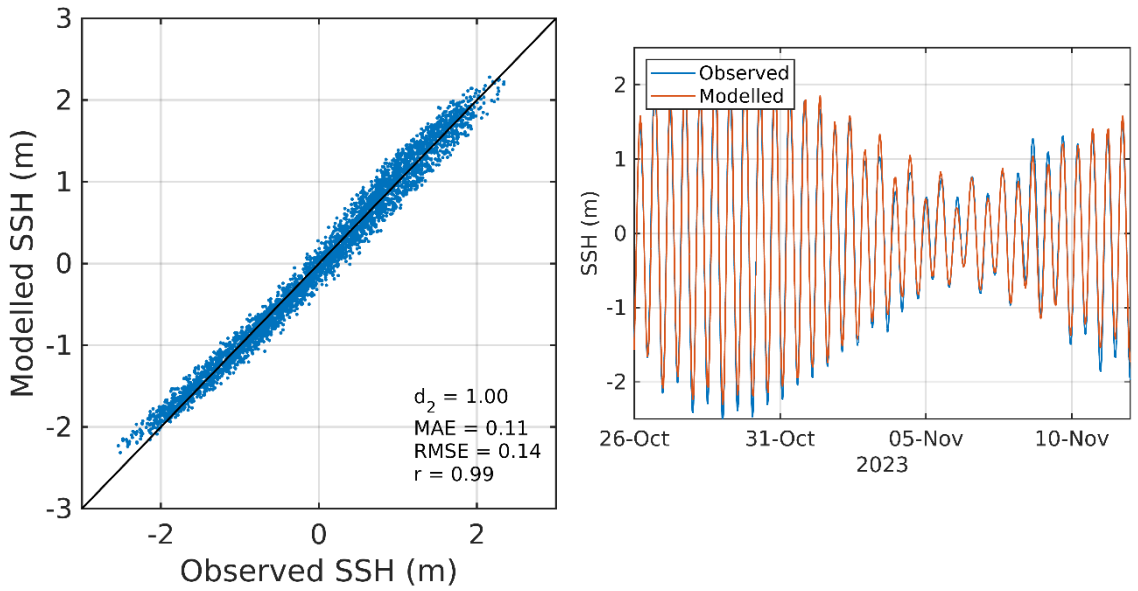

Figure 6. Comparison between observed and modelled sea surface height from 06 October – 29 November 2023 (ID424) using model parameter values from Table 1. Both the full record (left) and a subset of 15 days (right) are shown. Observed data are in blue, model results in red.

Table 2. Model performance statistics for sea surface height (SSH), and East and North velocity at the ADCP location for 06 October – 29 November 2023 (ID424) at three depths, 2.5 m, 6.0 m and 10.0m relative to the moving sea surface.

		Skill, d_2	MAE	RMSE
Sea Surface Height (SSH, m)		1.00	0.11	0.14
2.5 m	East Velocity (m s^{-1})	0.84	0.04	0.04
	North Velocity (m s^{-1})	0.70	0.04	0.05
6.0 m	East Velocity (m s^{-1})	0.64	0.03	0.04
	North Velocity (m s^{-1})	0.68	0.03	0.04
10.0 m	East Velocity (m s^{-1})	0.59	0.02	0.03
	North Velocity (m s^{-1})	0.73	0.02	0.03

North and East components of near-surface (2.5 m depth) velocity at the ADCP location were satisfactorily reproduced by the model, with values of the model skill, d_2, of 0.84 and 0.70 respectively (Figure 7, Table 2), and values of MAE and RMSE being in the range 0.04 – 0.05 m s^{-1} (Table 2). At the deeper cells (6.0 m and 10.0 m), model skill for both components of velocity were slightly less, in the range 0.59 – 0.73, but still at an acceptable level of accuracy given the challenges of accurately simulating current velocity. The MAE and RMSE values were in the range 0.02 – 0.04 m s^{-1}. The histograms and scatter plots shown in Figure 8 and Figure 9 demonstrate that the modelled currents were broadly of the same speed and direction as the observed data.

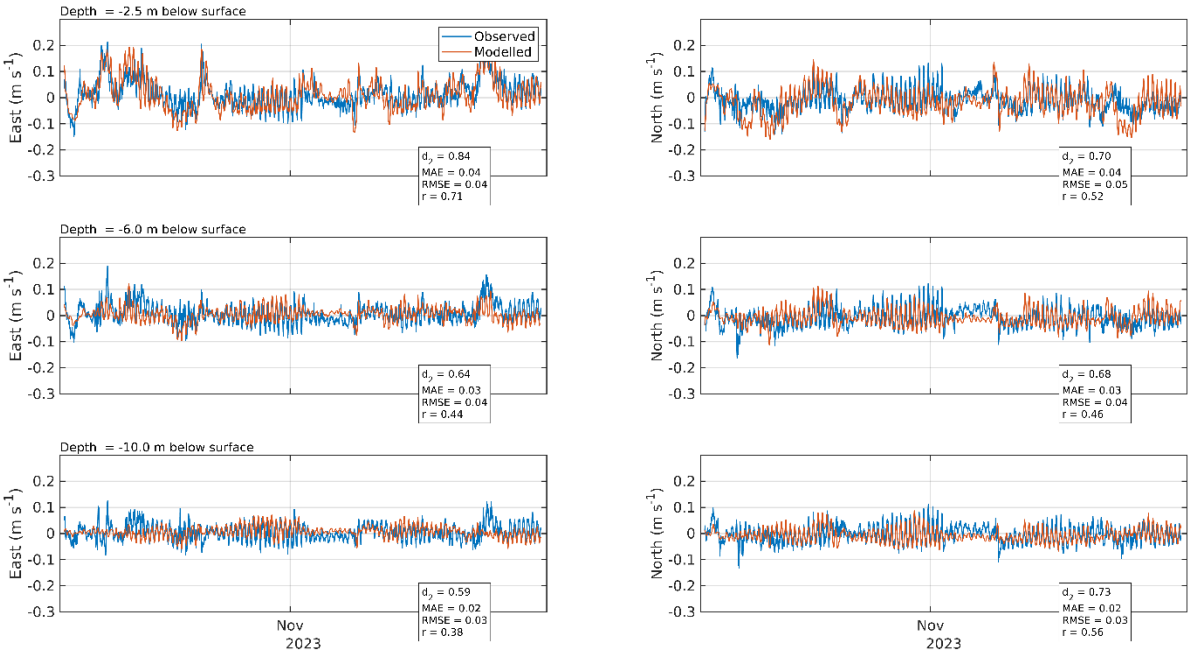

Figure 7. Comparison between observed and modelled East (left) and North (right) components of velocity at the ADCP location for 06 October – 29 November 2023 (ID424) at three depths, 2.5 m (top), 6.0 m and 10.0m (bottom) relative to the moving sea surface. Observed data are in blue, model results in red.

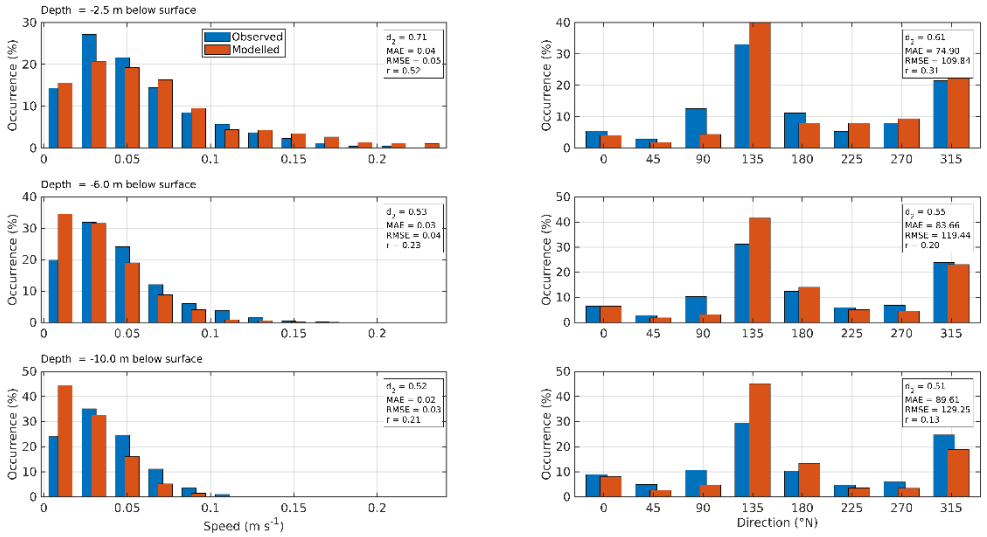

Figure 8. Histograms of observed and modelled speed (left) and direction (right) at the ADCP location for 06 October – 29 November 2023 (ID424) at three depths, 2.5 m (top), 6.0 m (middle) and 10.0m (bottom) relative to the moving sea surface. Observed data are in blue, model results in red.

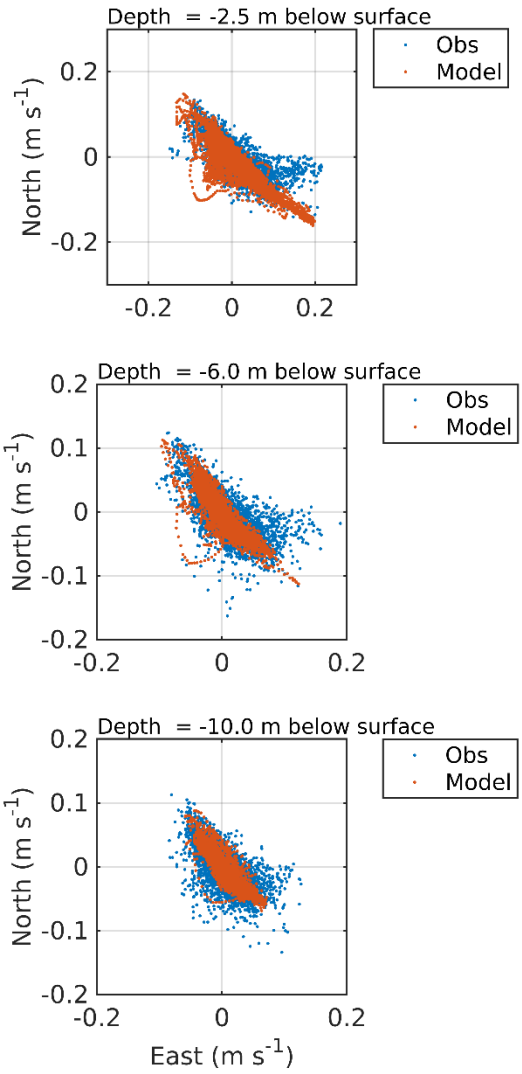

Figure 9. Scatter plot of observed and modelled velocity at the ADCP location for 06 October – 29 November 2023 (ID424) at three depths, 2.5 m (top), 6.0 m (middle) and 10.0m (bottom) relative to the moving sea surface. Observed data are in blue, model results in red.

4.3 Validation: 09 February – 07 May 2021 (ID367)

At the ADCP location, the sea surface height was reasonably modelled, with model skill of 0.99 (Figure 10, Table 3). The mean absolute error (MAE) and root-mean-square error (RMSE) values of 0.16 m and 0.20 respectively are about 3.6% and 4.4% of the spring tide range (4.5 m) respectively.

North and East components of near-surface (7.9m depth) velocity at the ADCP location were satisfactorily reproduced by the model, with values of the model skill, d_2, of 0.60 and 0.72 respectively (Figure 11, Table 3). The values of the MAE and RMSE were 3 – 4 cm s^{-1} (Table 3). At the deeper depth (17.9 m), the model skill, RMSE and MAE values were similar, with, in this case, slightly improved model performance near the seabed (43.9 m, Table 5). The histograms and scatter plots shown in Figure 12 and Figure 13 demonstrate that the modelled currents were broadly of the same speed and direction as the observed data.

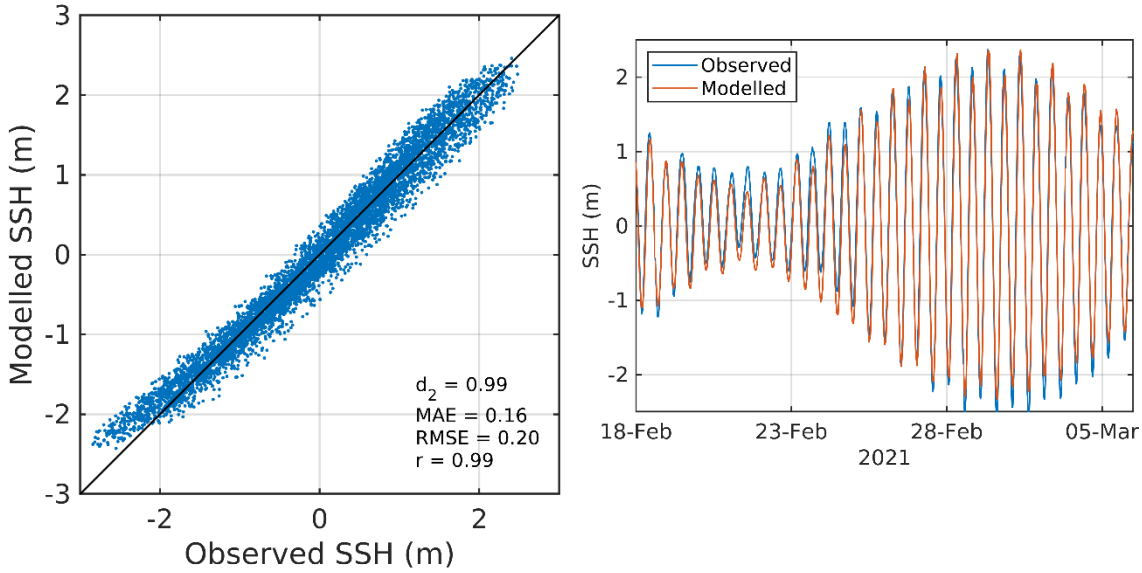

Figure 10. Comparison between observed and modelled sea surface height from 09 February – 07 May 2021 (ADCP deployment ID367) using model parameter values from Table 1. Both the full record (left) and a subset of 15 days (right) are shown. Observed data are in blue, model results in red.

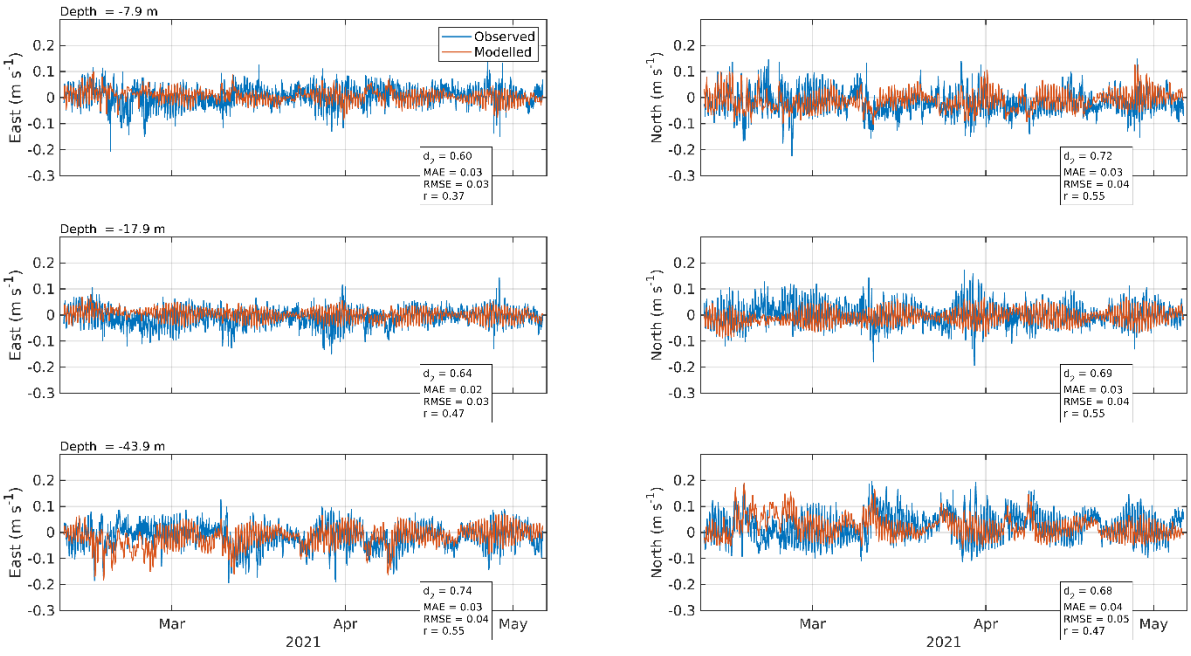

Figure 11. Comparison between observed and modelled East (left) and North (right) components of velocity at the ADCP location for 15 days in February 2021 (ID367) at three depths, 7.9 m, 17.9 m and 43.9 m. Observed data are in blue, model results in red.

Table 3. Model performance statistics for sea surface height (SSH), and East and North velocity at the ADCP location from 09 February – 07 May 2021 (ID367) at three depths, 7.9 m, 17.9 m and 43.9 m.

		Skill, d_2	MAE	RMSE
Sea Surface Height (SSH, m)		0.99	0.16	0.20
7.9 m	East Velocity (m s^{-1})	0.60	0.03	0.03
	North Velocity (m s^{-1})	0.72	0.03	0.04
17.9 m	East Velocity (m s^{-1})	0.64	0.02	0.03
	North Velocity (m s^{-1})	0.69	0.03	0.04
43.9 m	East Velocity (m s^{-1})	0.74	0.03	0.04
	North Velocity (m s^{-1})	0.68	0.04	0.05

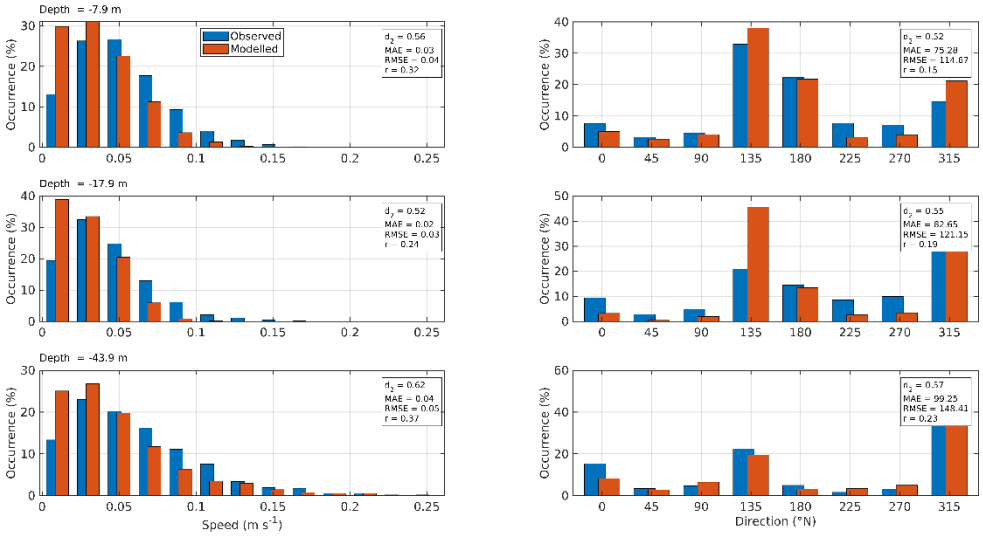

Figure 12. Histograms of observed and modelled current speed (left) and direction (right) at the ADCP location from 09 February – 07 May 2021 (ID367) at three depths, 7.9 m, 17.9 m and 43.9 m. Observed data are in blue, model results in red.

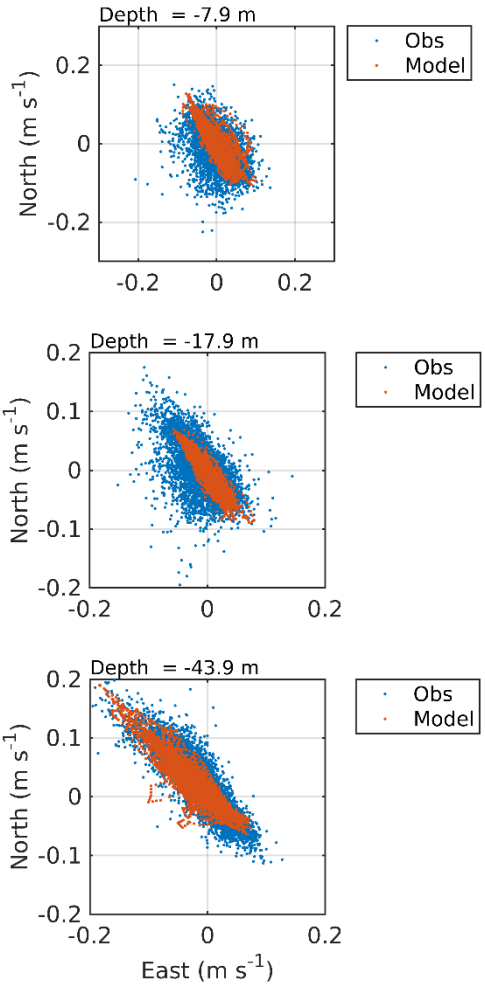

Figure 13. Scatter plot of observed and modelled velocity at the ADCP location from 09 February – 07 May 2021 (ID367) at three depths, 7.9 m, 17.9 m and 43.9 m. Observed data are in blue, model results in red.

4.4 Validation: 24 June – 10 September 2020 (ID346)

At the ADCP location, the sea surface height was well modelled, with model skill of 0.99 (Figure 14, Table 4). The mean absolute error (MAE) and root-mean-square error (RMSE) values of 0.13 m and 0.17 respectively are about 2.9% and 3.8% of the spring tide range (4.5 m) respectively.

Model skill scores were 0.56 and 0.59 for the East and North components of near-surface (6.9 m) velocity respectively, with MAE and RMSE values of 0.03 m s^{-1} and 0.04 m s^{-1} respectively for both components (Figure 15, Table 4). The values of d_2, MAE and RMSE for the deeper depths were similar to the near-surface values.

The histograms and scatter plots shown in Figure 16 and Figure 17 demonstrate that the modelled currents were broadly of the same speed and direction as the observed data.

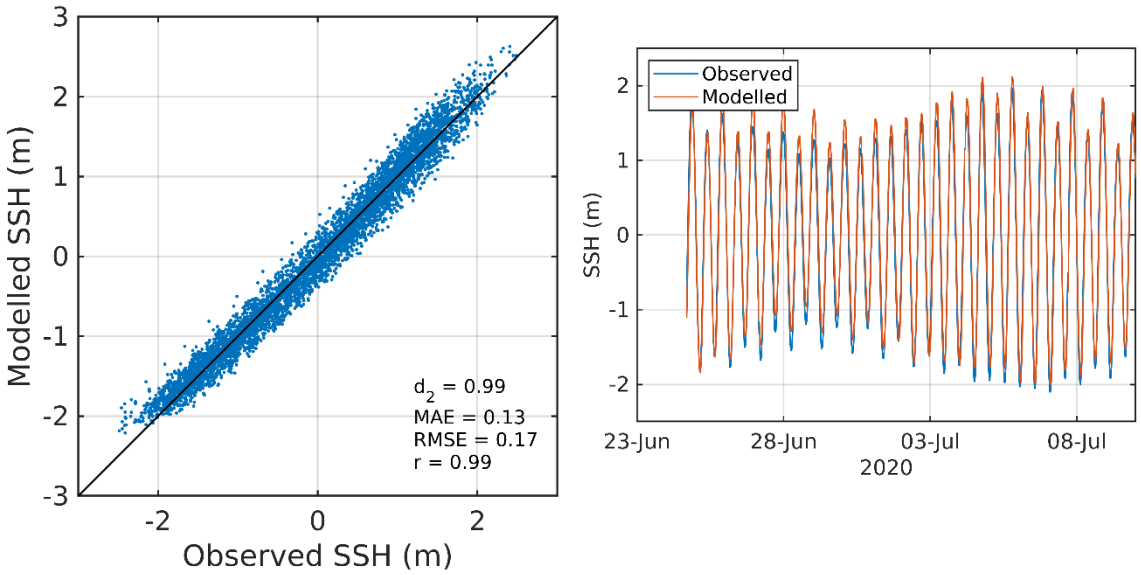

Figure 14. Comparison between observed and modelled sea surface height from 24 June – 10 September 2020 (ADCP deployment ID346) using model parameter values from Table 1. Both the full record (left) and a subset of 15 days (right) are shown. Observed data are in blue, model results in red.

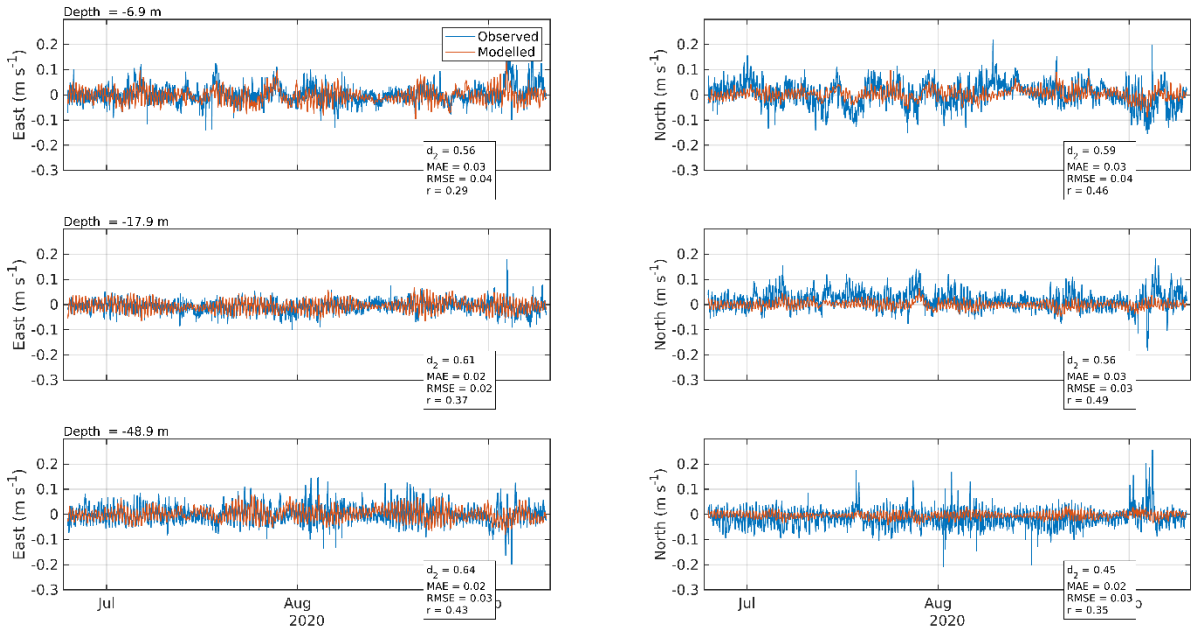

Figure 15. Comparison between observed and modelled East (left) and North (right) components of velocity at the ADCP location from 24 June – 10 September 2020 (ADCP deployment ID346) at three depths, 6.9m, 17.9 m and 48.9 m. Observed data are in blue, model results in red.

Table 4. Model performance statistics for sea surface height (SSH), and East and North velocity at the ADCP location from 24 June – 10 September 2020 (ADCP deployment ID346) at three depths, 6.9m, 17.9 m and 48.9 m.

		Skill, d_2	MAE	RMSE
Sea Surface Height (SSH, m)		0.99	0.13	0.17
6.9 m	East Velocity (m s^{-1})	0.56	0.03	0.04
	North Velocity (m s^{-1})	0.59	0.03	0.04
17.9 m	East Velocity (m s^{-1})	0.61	0.02	0.02
	North Velocity (m s^{-1})	0.56	0.03	0.03
48.9 m	East Velocity (m s^{-1})	0.64	0.02	0.03
	North Velocity (m s^{-1})	0.45	0.02	0.03

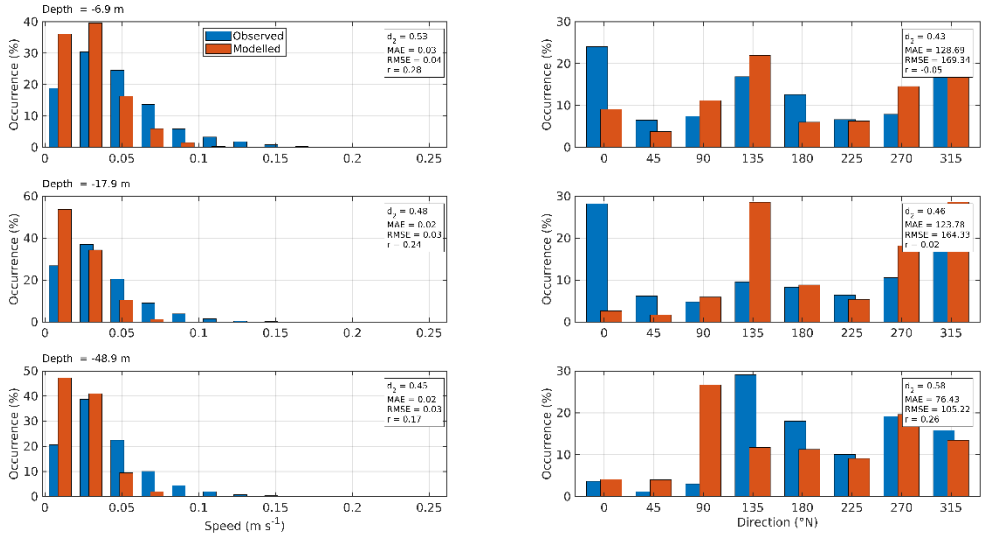

Figure 16. Histograms of observed and modelled current speed (left) and direction (right) at the ADCP location from 24 June – 10 September 2020 (ADCP deployment ID346) at three depths, 6.9m, 17.9 m and 48.9 m. Observed data are in blue, model results in red.

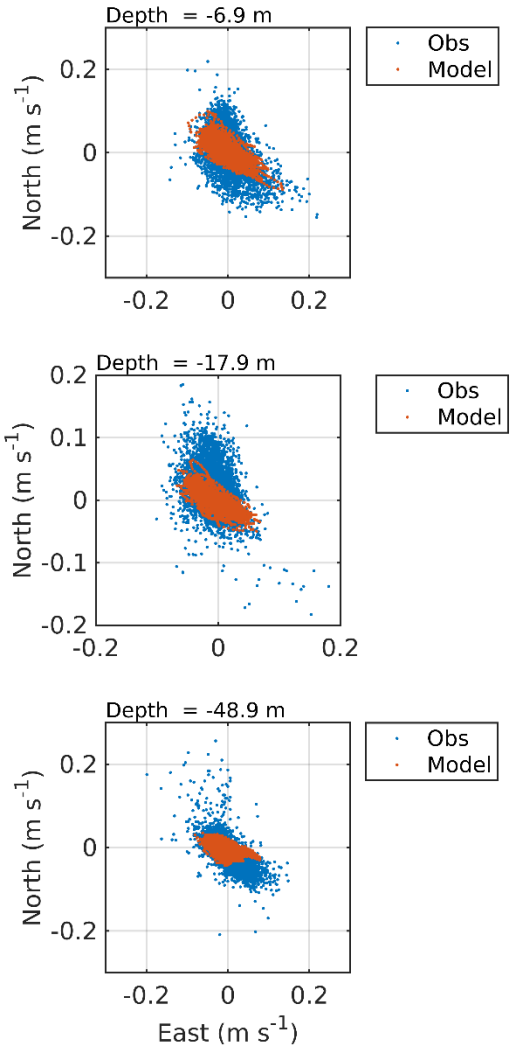

Figure 17. Scatter plot of observed and modelled velocity at the ADCP location from 24 June – 10 September 2020 (ADCP deployment ID346) at three depths, 6.9m, 17.9 m and 48.9 m. Observed data are in blue, model results in red.

4.5 Validation: 10 September – 08 November 2020 (ID357, ID358)

4.5.1 ID357

The results of the calibration exercise for ID357 are presented in Figure 18 – Figure 20 and Table 5. At the ADCP location, the sea surface height was accurately modelled, with model skill of 0.99. The mean absolute error (MAE) and root-mean-square error (RMSE) values of 0.17 m and 0.22 respectively are about 3.8% and 4.9% of the spring tide range (4.5 m) respectively.

For the calibration period, the model skill scores were 0.45 and 0.62 for the East and North components of near-surface (7.7 m) velocity respectively, with MAE and RMSE values in the range 0.03 m s^{-1} – 0.05 m s^{-1} for the two components of velocity (Table 5). At the deeper depth of 16.7 m, the skill scores were similar, at 0.57 and 0.59 respectively. The MAE and RMSE

values were slightly less than those at the shallower depth, at from 0.02 m s^{-1} – 0.04 m s^{-1}. Similar values were obtained for the near-bed results (Table 5).

The histograms and scatter plots (Figure 20 and Figure 21) demonstrate that the modelled current had broadly the same magnitude and direction characteristics as the observed data.

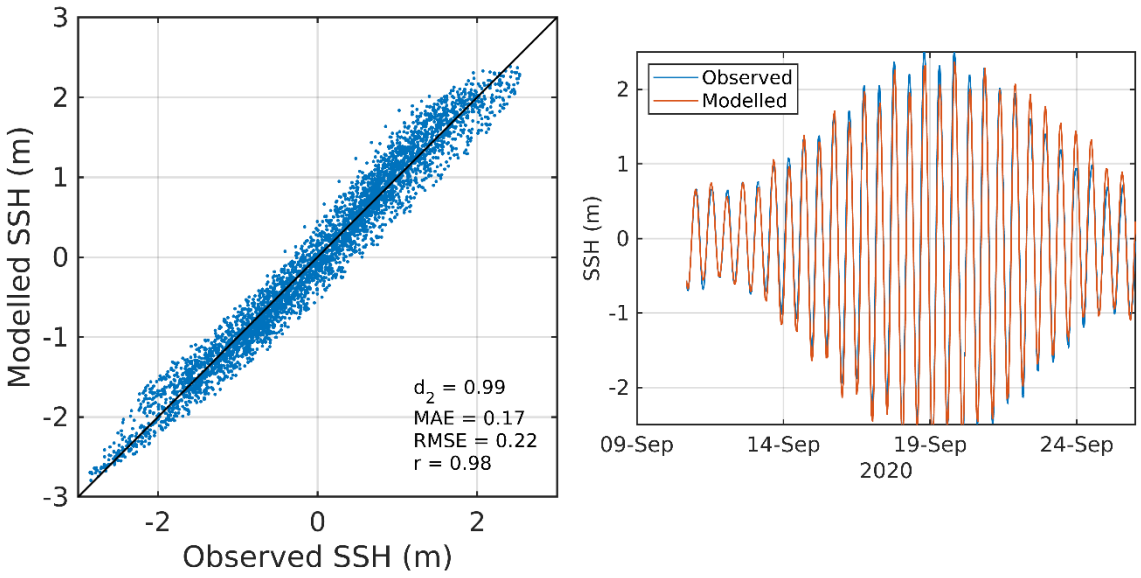

Figure 18. Comparison between observed and modelled sea surface height from ID357 using model parameter values from Table 1. Both the full record (left) and a subset of 15 days (right) are shown. In the latter, the observed data are in blue, model results in red.

Table 5. Model performance statistics for sea surface height (SSH) and East and North velocity at the ADCP location from 10 September – 08 November 2020 (ID357) at three depths (7.7 m, 16.7 m and 48.7 m).

		Skill, d_2	MAE	RMSE
Sea Surface Height (SSH, m)		0.99	0.17	0.22
7.7 m	East Velocity (m s^{-1})	0.45	0.03	0.04
	North Velocity (m s^{-1})	0.62	0.03	0.05
16.7 m	East Velocity (m s^{-1})	0.57	0.02	0.03
	North Velocity (m s^{-1})	0.59	0.03	0.04
48.7 m	East Velocity (m s^{-1})	0.73	0.02	0.03
	North Velocity (m s^{-1})	0.69	0.03	0.05

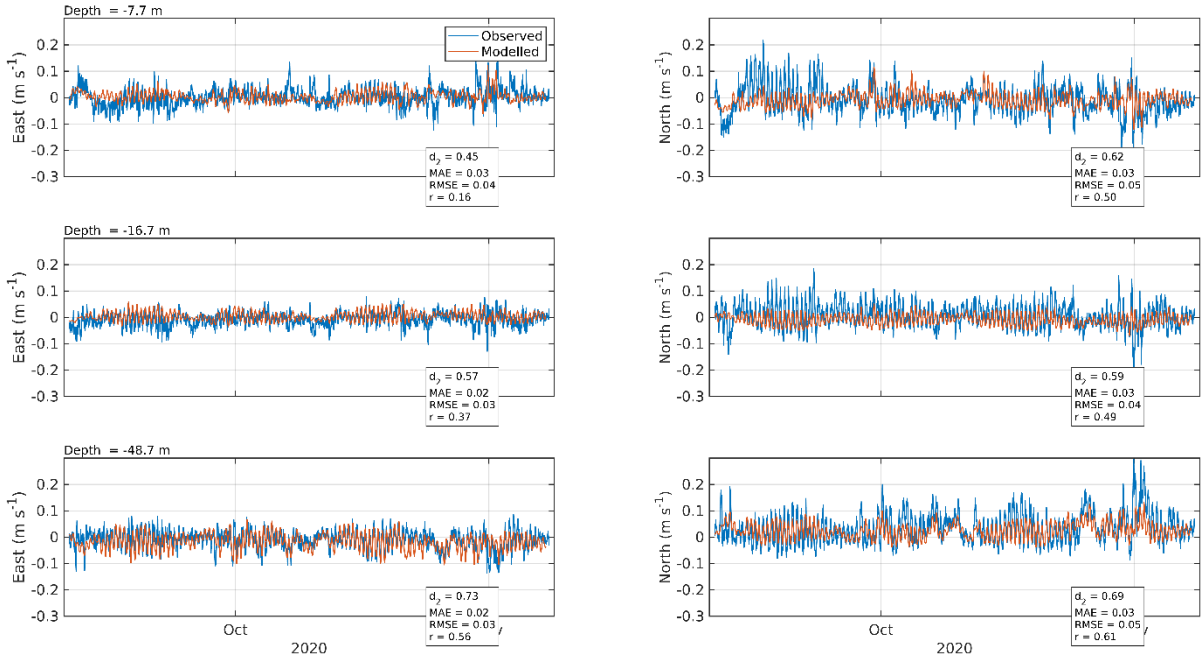

Figure 19. Comparison between observed and modelled East (left) and North (right) components of velocity at the ADCP from 10 September – 08 November 2020 (ID357) at three depths: 7.7m (top), 16.7 m (middle) and 48.7m (bottom). Observed data are in blue, model results in red.

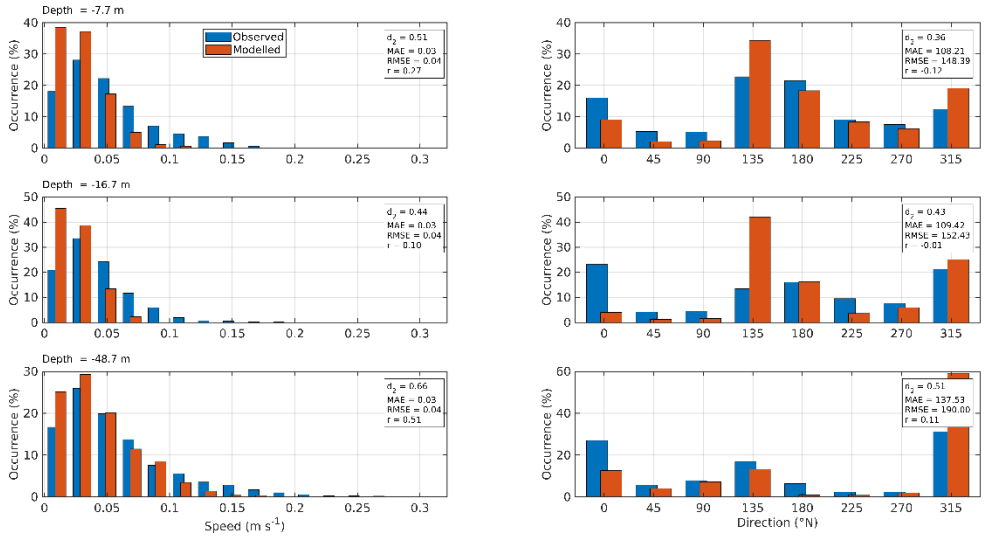

Figure 20. Histograms of observed and modelled speed (left) and direction (right) at the ADCP location from 10 September – 08 November 2020 (ID357) at three depths: 7.7m (top), 16.7 m (middle) and 48.7m (bottom). Observed data are in blue, model results in red.

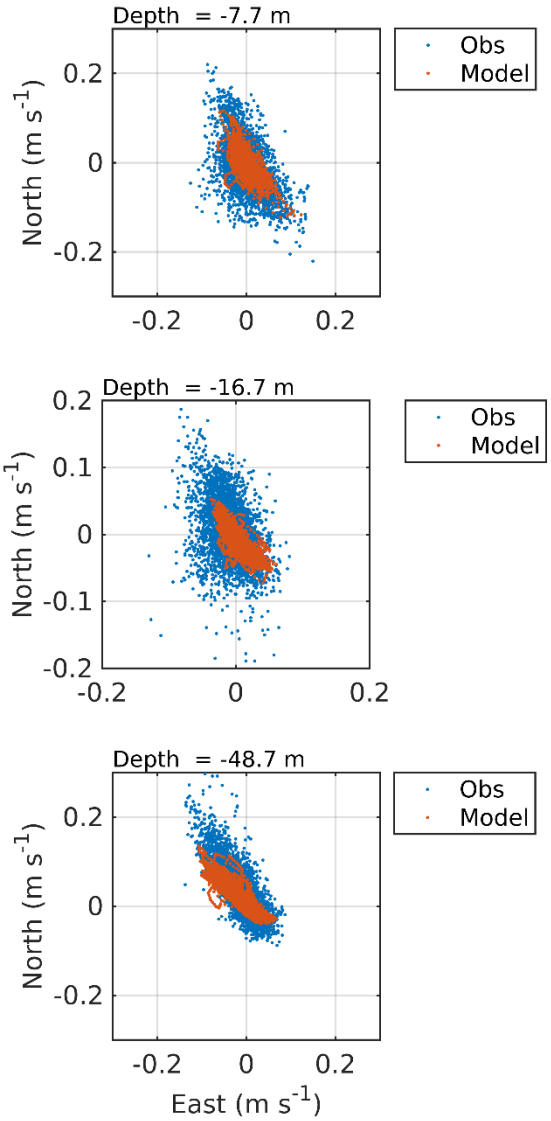

Figure 21. Scatter plot of observed and modelled velocity at the ADCP location from 10 September – 08 November 2020 (ID357) at three depths: 7.7m (top), 16.7 m (middle) and 48.7m (bottom). Observed data are in blue, model results in red.

4.5.2 ID358

The results of the calibration exercise for ID358 are presented in Figure 22 – Figure 25 and Table 6. At the ADCP location, the sea surface height was accurately modelled, with model skill of 0.99. The mean absolute error (MAE) and root-mean-square error (RMSE) values of 0.17 m and 0.22 respectively are about 3.8% and 4.9% of the spring tide range (4.5 m) respectively.

For the calibration period, the model skill scores were 0.62 and 0.60 for the East and North components of near-surface (7.4 m) velocity respectively, with RMSE values of 0.04 m s^{-1} and 0.03 m s^{-1} for the two components of velocity respectively (Table 6). At the deeper depth of 14.4 m, the skill scores were similar, at 0.62 and 0.55 respectively; the MAE and RMSE values

were less than those at the shallower depth, in the range 0.02 m s^{-1} – 0.03 m s^{-1}. The skill scores and errors for the near-bed velocity were similar (Table 6).

The histograms and scatter plots (Figure 24 and Figure 25) demonstrate that the modelled current had broadly the same magnitude and direction characteristics as the observed data.

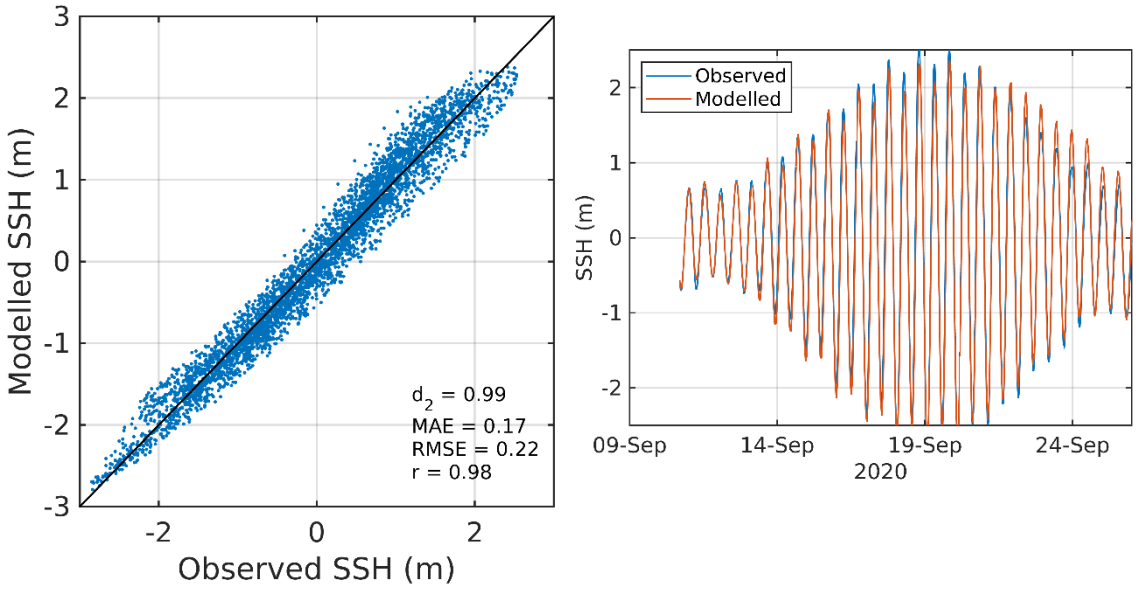

Figure 22. Comparison between observed and modelled sea surface height from ID358 using model parameter values from Table 1. Both the full record (left) and a subset of 15 days (right) are shown. In the latter, the observed data are in blue, model results in red.

Table 6. Model performance statistics for sea surface height (SSH) and East and North velocity at the ADCP location from 10 September – 08 November 2020 (ID358) at three depths (7.4 m, 14.4 m and 46.4 m).

		Skill, d_2	MAE	RMSE
Sea Surface Height (SSH, m)		0.99	0.17	0.22
7.4 m	East Velocity (m s^{-1})	0.61	0.03	0.04
	North Velocity (m s^{-1})	0.60	0.02	0.03
14.4 m	East Velocity (m s^{-1})	0.62	0.02	0.03
	North Velocity (m s^{-1})	0.55	0.02	0.03
46.4 m	East Velocity (m s^{-1})	0.74	0.03	0.04
	North Velocity (m s^{-1})	0.47	0.02	0.02

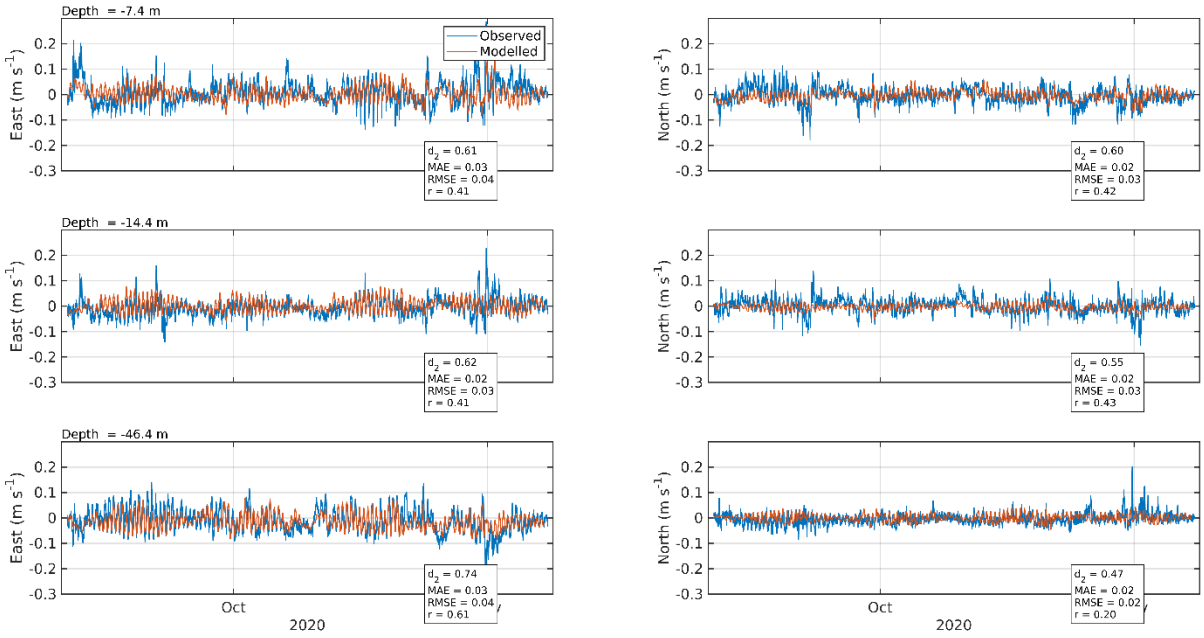

Figure 23. Comparison between observed and modelled East (left) and North (right) components of velocity at the ADCP location from 10 September – 08 November 2020 (ID358) at three depths: 7.4m (top), 14.4 m (middle) and 46.4m (bottom). Observed data are in blue, model results in red.

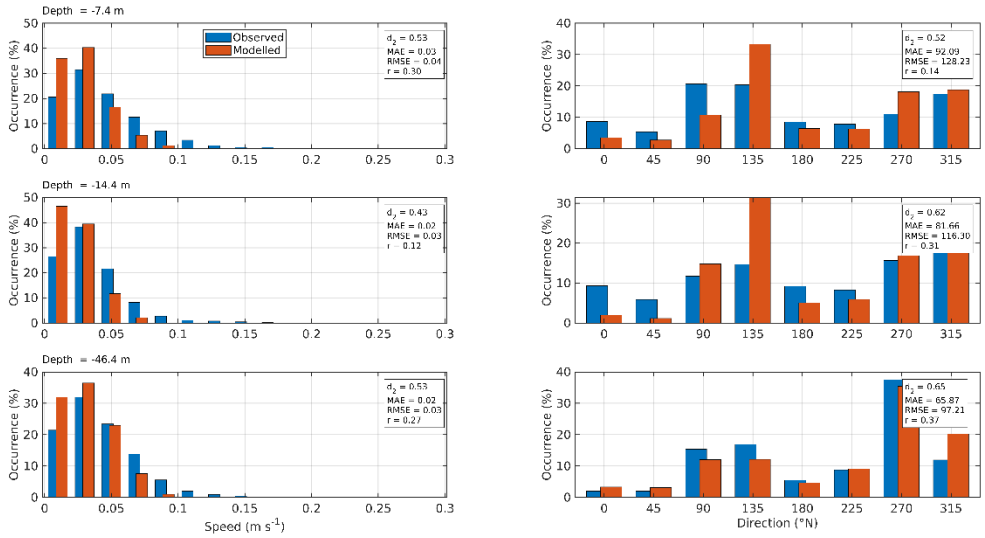

Figure 24. Histograms of observed and modelled speed (left) and direction (right) at the ADCP location from 10 September – 08 November 2020 (ID358) at three depths: 7.4m (top), 14.4 m (middle) and 46.4m (bottom). Observed data are in blue, model results in red.

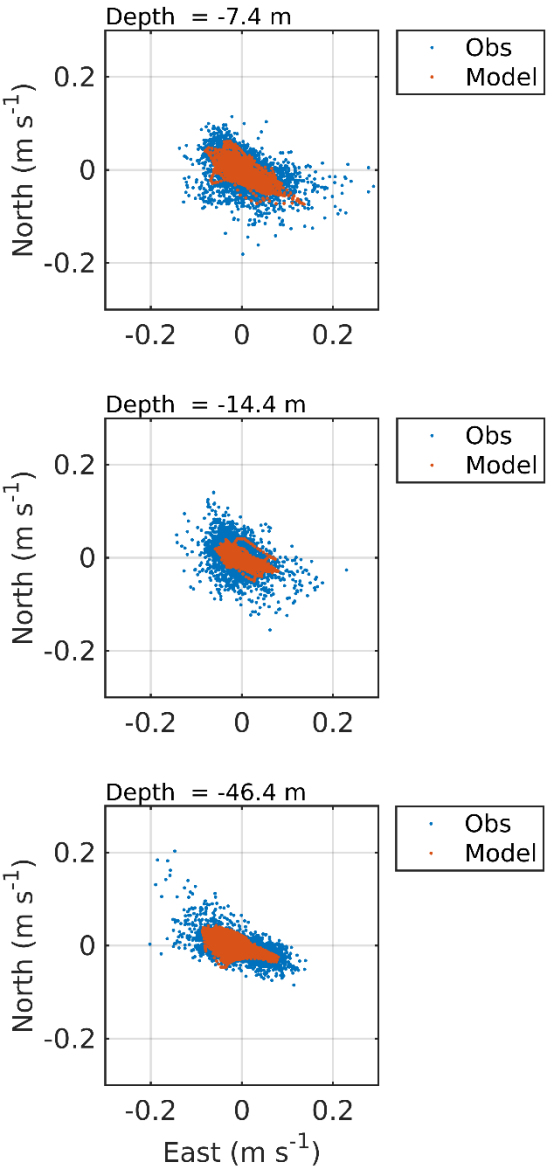

Figure 25. Scatter plot of observed and modelled velocity at the ADCP location from 10 September – 08 November 2020 (ID358) at three depths: 7.4m (top), 14.4 m (middle) and 46.4m (bottom). Observed data are in blue, model results in red.

5. Modelled Flow Fields

Modelled flood and ebb velocity vectors at spring tides are illustrated in Figure 26. Modelled near-surface (model layer 2, σ = -0.05) current speeds in outer Loch Shell at springs were typically in the range 5 – 30 cm s^{-1}, being stronger on the ebb tide than on the flood, as expected in a stratified sea loch, and also stronger through the constrained channel sections with the loch. Modelled currents speeds were weaker during neap tides.

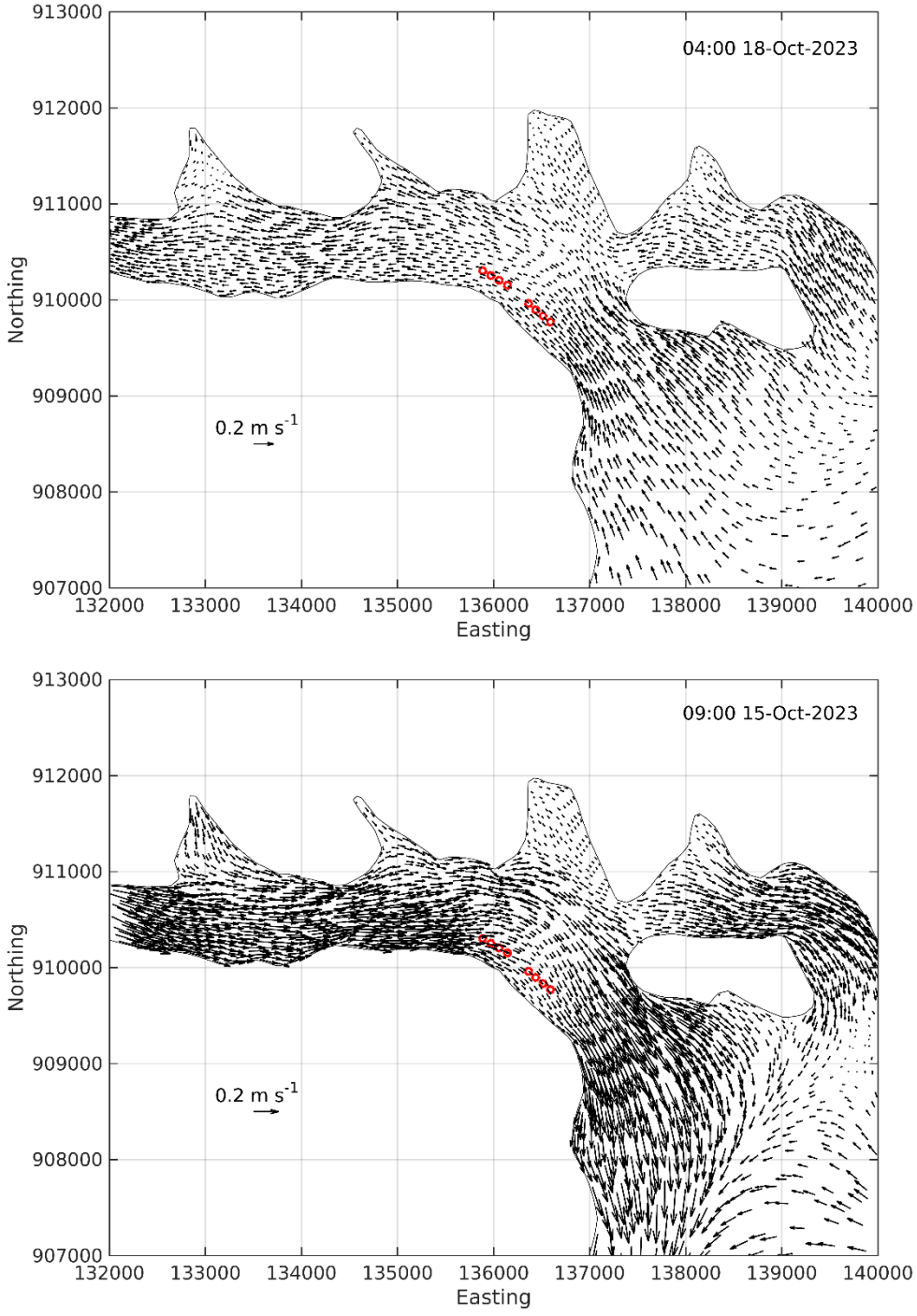

*Figure 26. Modelled flood (top) and ebb (bottom) sub-surface (model layer 2) current vectors during spring tides on 18th and 15th October 2023 respectively. For clarity, only 20% of the model vectors are shown. Pen locations are indicated (**O**).*

The mean (residual) sub-surface currents were seaward within Loch Shell (Figure 27), again as expected in a stratified sea loch. The model indicates a weaker circulation around the north of the island of Eilean Liubhaird. These residual flows indicate that the net transport of patches

of medicine following treatment at the Caolas a Deas sites will be eastward into the open waters of the Minch, where dispersion and dilution is likely to be rapid.

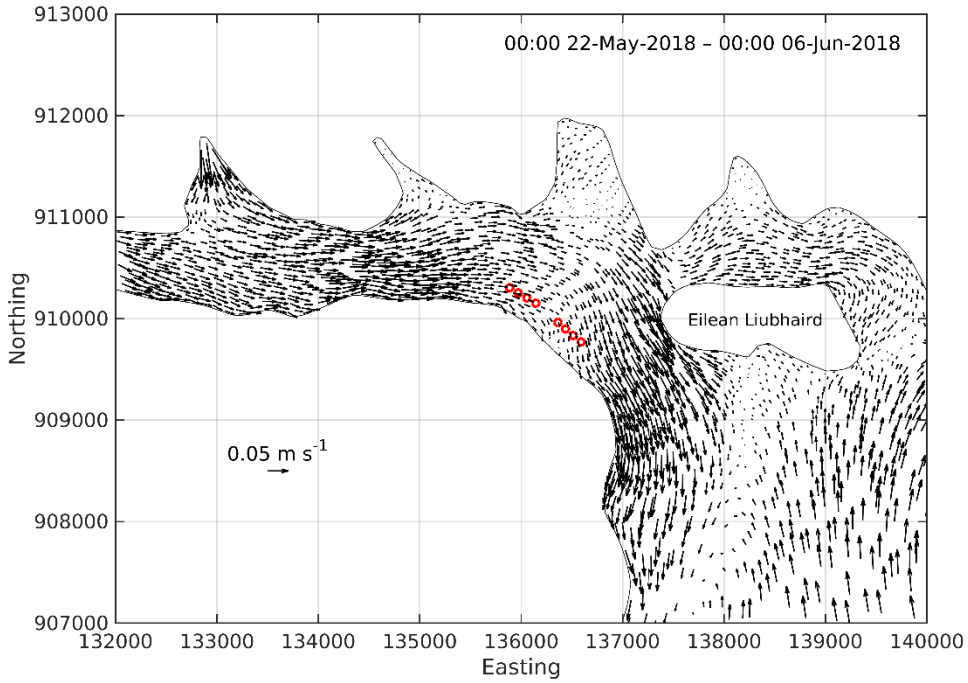

*Figure 27. Modelled mean (residual) sub-surface (model layer 2) current vectors averaged over the full simulation from 6th October – 30th November 2023. For clarity, only 20% of the model vectors are shown. Pen locations are indicated (**O**).*

6. Model Evaluation against Dye & Drogue Track Data

Anderson Marine Surveys Ltd. undertook a number of dye and drogue studies at the Caolas a Deas sites in outer Loch Shell in July 2020. The times and locations of the dye releases are detailed in Table 7. For each release, *ca.* 1 kg of dye was discharged.

Table 7. Details of the dye releases undertaken at Caolas a Deas in July 2020.

Release	Date	Release Time	Easting	Northing
1	23/07/2020	05:57:35	136466	910116
2	23/07/2020	09:52:20	136696	909721
3	23/07/2020	11:52:30	136704	909723
4	23/07/2020	12:59:55	136678	909709
5	23/07/2020	16:00:26	136713	909713

Following each release, multiple discrete surveys of the dye patch were undertaken. From these data, the location of the centre of the dye patch was estimated over time. However, tracking of the third dye patch was abandoned due to an insufficient quantity of dye being released to track, so only results from releases 1, 2, 4 and 5 are shown here.

The modelling simulated these releases by releasing 10,000 particles in discrete patches at the times given in Table 7. Modelled particle locations were recorded every 5 minutes, and the **mean** particle location (assumed to represent the centre of the patch) was calculated. Particles were released in a 10 m radius circle about the release location over a depth range of 0 – 1 m. The tracks of the modelled mean patch centres were then compared to the observed data tracks.

The drogue releases were carried out simultaneously with the dye releases, using standard-pattern drogues with a reduced sail depth (≈1 m, due to relatively shallow water depths), fitted with GlobalSat GPS dataloggers recording at 2 min intervals. Release and recovery times and release positions are given in Table 8. Four drogues were used at each release.

Figure 28 shows the modelled and observed dye tracks for the releases detailed in Table 7 and confirms that the model broadly matches the tracks of the observed dye tracks for all eight releases.

Table 8. Details of the drogue releases undertaken at Caolas a Deas in outer Loch Shell in July 2020.

Release No.	Date	Release Time	Recovery Time	Easting	Northing
1	23/07/2020	05:59	09:42	136477	910112
2	23/07/2020	09:54	11:40	136699	909720
3	23/07/2020	11:54	13:20	136716	909703
4	23/07/2020	13:32	15:47	136701	909710
5	23/07/2020	16:02	16:55	136748	909686

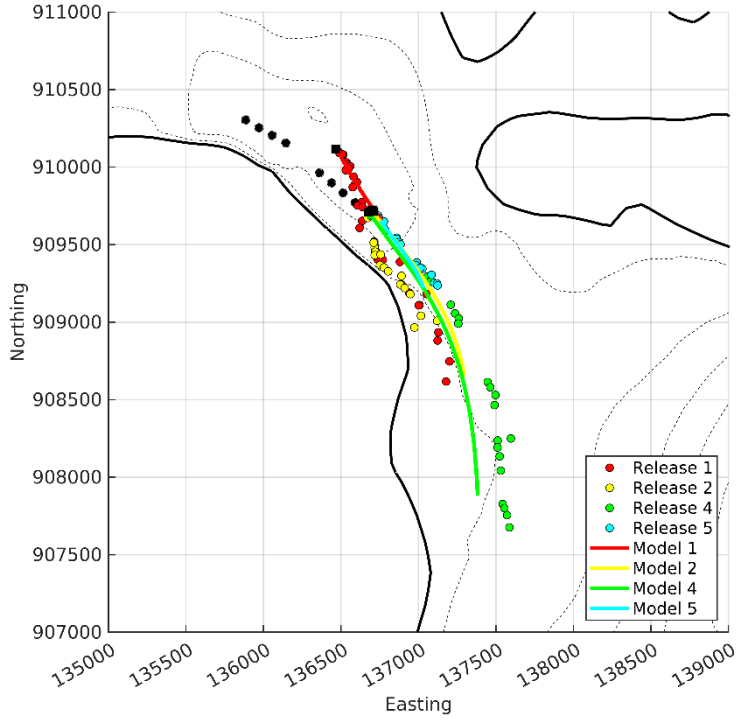

Figure 28. Observed (points) and modelled (solid lines) dye tracks for the four successful dye releases at Caolas a Deas on the 23rd July 2020. The dye release locations (■) and pen locations (●) are indicated.

The modelling simulated the drogue releases in a similar way to the dye patches. Ten thousand particles were used to simulate each drogue release, and the mean particle location calculated to represent the “numerical drogue” location. Modelled particle locations were recorded every 5 minutes, and the mean particle location (assumed to represent the drogue location) was calculated. Particles were released in a 10 m radius circle about the release location at a fixed depth 1 m. The tracks of the modelled drogues were then compared to the observed data tracks. Figure 29 shows the modelled and observed drogue tracks for the releases detailed in Table 8 and confirms that the model broadly matches the tracks of the observed drogues in all instances, concluding that the model is fit-for-purpose to model dispersion of bath medicines.

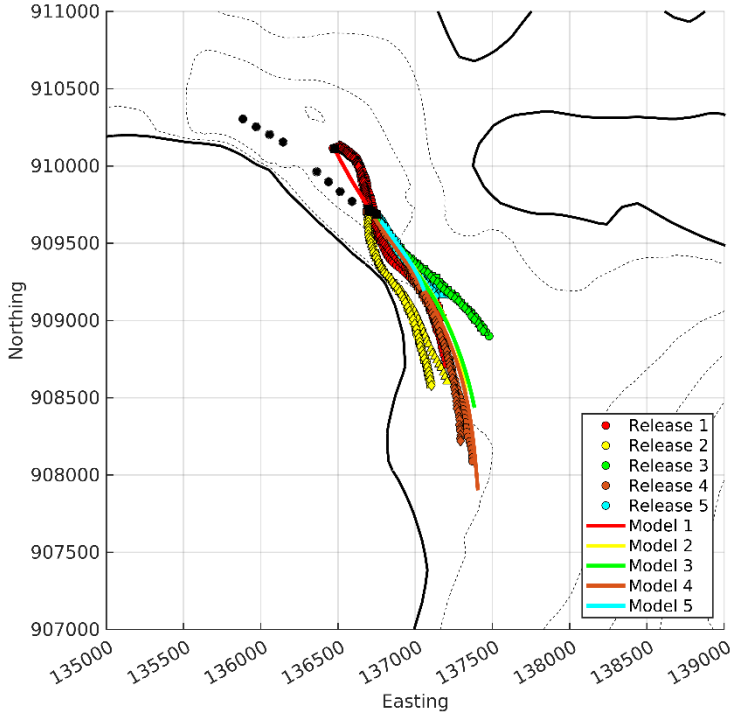

Figure 29. Observed (points) and modelled (solid lines) drogue tracks from the five releases at Caolas a Deas on 23rd July 2020. The different shaped points (○, ◊, □, Δ) represent individual drogues, while the colouring indicates the release number. The drogue release locations (■) and pen locations (●) are indicated.

7. References

Aleynik, D. Davidson, K., Dale A. C. and Porter, M., 2016. A high resolution hydrodynamic model system suitable for novel harmful algal bloom modelling in areas of complex coastline and topography. Harmful Algae, 53(3):102–117, 10.1016/j.hal.2015.11.012

Burchard, H., 2002. Applied turbulence modelling in marine waters. Springer:Berlin-Heidelberg-New York-Barcelona-Hong Kong-London-Milan Paris-Tokyo, 215pp.

Chen, C., H. Liu, and R.C. Beardsley, 2003. An unstructured, finite-volume, three-dimensional, primitive equation ocean model: Application to coastal ocean and estuaries. J. Atmos. Ocean. Tech., 20, 159 – 186.

de Dominicis, M., O'Hara Murray, R., Wolf, J. Gallego, A. (2018) The Scottish Shelf Model 1990 – 2014 climatology – reduced precision output from version 2.01. doi: 10.7489/12122-1

Gillibrand, P.A., Walters, R.A., and McIlvenny, J., 2016. Numerical simulations of the effects of a tidal turbine array on near-bed velocity and local bed shear stress. *Energies*, vol 9, no. 10, pp. 852. DOI: 10.3390/en9100852

Large. W.G. and Pond, S., 1981. Open ocean momentum flux measurements in moderate to strong winds. J. Phys. Oceanogr., 11, 324—336.

Mellor, G. L. and Yamada, T., 1982. Development of a turbulence closure model for geophysical fluid problem. Rev. Geophys. Space. Phys., 20, 851-875.

Mowi Scotland Ltd. 2024a. Caolas a Deas West, Loch Shell, Bath Medicine Dispersion Modelling Report, April 2024, 34 pp.

Mowi Scotland Ltd. 2024b. Caolas a Deas East, Loch Shell, Bath Medicine Dispersion Modelling Report, April 2024, 34 pp.

Price, D., Stuiver, C., Johnson, H., Gallego, A., O' Hara Murray, R., 2016. The Scottish Shelf Model. Part 4: East Coast of Lewis and Harris Sub-Domain. Scottish Marine and Freshwater Science Vol 7 No 6, 147 pp.

SEPA, 2023. Interim Marine Modelling Guidance for Aquaculture Applications. Scottish Environment Protection Agency, December 2023, 11 pp.

Walters, R.A.; Casulli, V., 1998. A robust, finite element model for hydrostatic surface water flows. Comm. Num. Methods Eng., 14, 931–940.

Willmott, C. J.; Ackleson, S. G.; Davis, R. E.; Feddema, J. J.; Klink, K. M.; Legates, D. R. O'Donnell, J.; Rowe, C. M. 1985. Statistics for evaluation and comparison of models, J. Geophys. Res., 90, 8995– 9005.